Annales Geophysicae (2004) 22: 4089–4101
SRef-ID: 1432-0576/ag/2004-22-4089

Annales Geophysicae

Temporal evolution of two auroral arcs as measured by the Cluster satellite and coordinated ground-based instruments

A. T. Aikio[1], K. Mursula[1], S. Buchert[2], F. Forme[3], O. Amm[4], G. Marklund[5], M. Dunlop[6], D. Fontaine[3], A. Vaivads[2], and A. Fazakerley[7]

[1]University of Oulu, Department of Physical Sciences, P.O. Box 3000, FIN-90014 University of Oulu, Finland
[2]Swedish Institute of Space Physics, Angströmlaboratoriet, Box 534, SE 75121 Uppsala, Sweden
[3]CETP/UVSQ, 10-12 Av de l'europe, 78140 Velizy, France
[4]Finnish Meteorological Institute, Geophysical Research, P.O. Box 503, FIN-00101 Helsinki, Finland
[5]Division of Plasma Physics, Alfvén Laboratory, Royal Institute of Technology, S-100 44, Stockholm, Sweden
[6]Imperial College, Blackett Laboratory, Space and Atmospheric Physics Group, London SW7 2BZ, UK
[7]Mullard Space Science Laboratory, University College, London, UK

Received: 21 November 2003 – Revised: 24 August 2004 – Accepted: 3 September 2004 – Published: 22 December 2004

Abstract. The four Cluster s/c passed over Northern Scandinavia on 6 February 2001 from south-east to north-west at a radial distance of about 4.4 R_E in the post-midnight sector. When mapped along geomagnetic field lines, the separation of the spacecraft in the ionosphere was confined to within 110 km in latitude and 50 km in longitude. This constellation allowed us to study the temporal evolution of plasma with a time scale of a few minutes. Ground-based instrumentation used involved two all-sky cameras, magnetometers and the EISCAT radar. The main findings were as follows.

Two auroral arcs were located close to the equatorward and poleward edge of a large-scale density cavity, respectively. These arcs showed a different kind of a temporal evolution. (1) As a response to a pseudo-breakup onset, both the up- and downward field-aligned current (FAC) sheets associated with the equatorward arc widened and the total amount of FAC doubled in a time scale of 1–2 min. (2) In the poleward arc, a density cavity formed in the ionosphere in the return (downward) current region. As a result of ionospheric feedback, a strongly enhanced ionospheric southward electric field developed in the region of decreased Pedersen conductance. Furthermore, the acceleration potential of ionospheric electrons, carrying the return current, increased from 200 to 1000 eV in 70 s, and the return current region widened in order to supply a constant amount of return current to the arc current circuit.

Evidence of local acceleration of the electron population by dispersive Alfvén waves was obtained in the upward FAC region of the poleward arc. However, the downward accelerated suprathermal electrons must be further energised below Cluster in order to be able to produce the observed visible aurora.

Both of the auroral arcs were associated with broad-band ULF/ELF (BBELF) waves, but they were highly localised in space and time. The most intense BBELF waves were confined typically to the return current regions adjacent to the visual arc, but in one case also to a weak upward FAC region. BBELF waves could appear/disappear between s/c crossings of the same arc separated by about 1 min.

Key words. Ionosphere (electric fields and currents) – Magnetospheric physics (auroral phenomena; magnetosphere-ionosphere interactions)

Correspondence to: A. T. Aikio
(anita.aikio@oulu.fi)

1 Introduction

Satellite and rocket observations in the auroral zone below and within the auroral acceleration region have been performed by many spacecraft since the discovery of the region in the 1970's (Mozer et al., 1977). The acceleration region can be located at altitudes from the vicinity of the upper boundary of the ionosphere to several Earth radii and the acceleration region has been studied, for example, by the S3-3, DE-1, Viking, Akebono, Freja, FAST and Polar satellites; see reviews, e.g. by Lundin and Eliasson (1991), McFadden et al. (1999), Marklund and Karlsson (2001) and Olsson and Janhunen (2003). Electric field and particle observations have shown that auroras are often accompanied by a quasi-static upward electric field at high altitudes, which accelerates electrons downward and ions upward. High-resolution observations in the 1990's revealed that a reverse signature can be observed in return current regions: upward flowing energetic electron beams, which appear to be accelerated by a quasi-static downward electric field (Marklund et al., 1994; Carlson et al., 1998a). Within and above the acceleration region, various wave modes are also observed, for example, EMIC and EIC waves, which can interact with electrons (McFadden

et al., 1999). On auroral field lines, broad-band ULF/ELF electric field fluctuations are commonly observed, discussed more in Sect. 4.2.

In this paper, the satellite observations of the arcs were made at an altitude of about 22 000 km (corresponding to a radial distance of 4.4 R_E). The four Cluster spacecraft (C1–C4) were flying over Northern Scandinavia from south-east to north-west in the post-midnight sector (at about 01:40 MLT). When mapped along the geomagnetic field lines, the separation of the spacecraft in the ionosphere was confined to within 110 km in latitude and 50 km in longitude. This constellation allows us to study the temporal evolution of plasma with a time scale of a few minutes. In this study, data from three spacecraft (C1, C2 and C4) are available, since instruments at Cluster 3 were switched on later. The meso-scale structures of the same Cluster pass were studied by Amm et al. (2003) and according to that study the part of the orbit studied here (geographic latitudes below 70°) was located in the region of the large-scale westward electrojet (WEJ), equatorward of the convection reversal and the open-closed field line boundary, which was situated 3–4° poleward of the convection reversal. In this paper, we use coordinated ground-based and satellite observations to study the evolution of two auroral arcs. The ground-based data were measured by two all-sky cameras, the EISCAT (European incoherent Scatter) radar and magnetometers. The advantages of having ground-based observations are several. The evolution of optical aurora is known for a longer time interval and from a wider spatial region. Ground observations allow for the determination of arc velocities, which affect the current density values calculated from the satellite magnetometer data. Optical observations also help to separate pure temporal changes from those caused by motion of structures, especially in the direction perpendicular to the s/c trajectory.

2 Instrumentation

The ground projection of the Cluster s/c along the magnetic field lines according to the T89c K_p=3 model (Tsyganenko, 1989), is shown in Fig. 1. From this figure one can see that Cluster 1 and 3 form a pair and Cluster 2 and 4 another pair, which follow almost the same orbit on the ground (the "string of pearls" configuration). The orbits are separated only by about 50 km in geographic longitude and the instantaneous separation in latitude is about 1° between C1 and C4. Data from C3 was not available for the time of interest here.

The T89c model with K_p=3 provides good mapping for the more equatorward arc, but for the poleward arc we must use K_p=5 obtain good agreement with the optical observations. This change can be justified by an onset of a pseudo-breakup between the two arc crossings.

We have utilised measurements from three Cluster instruments: the Electric Field and Wave Instrument, EFW (Gustafsson et al., 1997), the Fluxgate Magnetometer, FGM (Balogh et al., 1997) and the Plasma Electron And Current Experiment, PEACE (Johnstone et al., 1997). Since the EFW instrument measures the electric field by two pairs of probes in the spin plane, the measurement provides only two components of the electric field. The third component can be calculated by assuming that the electric field along the main magnetic field vanishes, which is usually a good approximation. However, when the magnetic field is confined on or near the spin plane, the calculation can't be done. This happens during the crossing of the more poleward arc. The DC electric field is calculated as a spin fit to a probe-pair measurement with 4-s resolution and it is presented in the FAC (field-aligned) coordinate system, where the positive Z-axis points in the direction of the Earth's magnetic field at the spacecraft's location, the positive X-axis lies in the plane of the Earth's magnetic field line, perpendicular to the Z-axis, and points inwards, i.e. towards the magnetic equator and the positive Y-axis completes the orthogonal right-handed system (it points towards west during the studied time interval).

To study the electric field fluctuations, we use high time resolution, 450 samples/s, electric field data from the EFW instrument. These data are presented in the BSC (Magnetic Spacecraft Coordinates) coordinate system, where the Z-axis is along the satellite spin axis, the X-axis is along the projection of the magnetic field vector on the spin plane and the Y-axis closes the right-handed coordinate system.

Data from the FGM instrument is used to calculate the field-aligned current (FAC) densities for each s/c separately. The contribution of the Earth's average geomagnetic field is subtracted from the spin-resolution (4 s) measurement and the remaining variations are fitted to the magnetic field of infinite current sheets with variable orientation. However, it turned out that the current sheets were nearly east-west aligned.

The PEACE instrument was switched on between the two arc crossings and we will show data from the HEEA (High-Energy Electron Analyser) sensor covering the energy range from 36.2 eV to 23.7 keV. The full 4π solid angle coverage is composed of a grid of 12 polar bins by 32 azimuthal bins; each bin is 15° by 11.25°. The data are acquired simultaneously in all 12 polar bins while the azimuthal data are gathered as the satellite spins.

Optical data were measured by the all-sky cameras (ASCs) of the MIRACLE network, Sodankylä, SOD (67.37° N, 26.63° E geographic) and Abisko, ABK (68.36° N, 18.82° E geographic). The temporal resolution of both of the instruments was 20 s and we have used the most intense wavelength of the event, 557.7 nm, in the figures shown.

EISCAT was making field-aligned measurements at Tromsø in the field-aligned CP1L mode, poleward of the two arcs, but within the downward return current region of the poleward arc. The EISCAT radar provided estimates of plasma parameters, such as electron density, electron and ion temperature and ion velocity. The electric field vector could not be determined because of technical problems at the two remote sites.

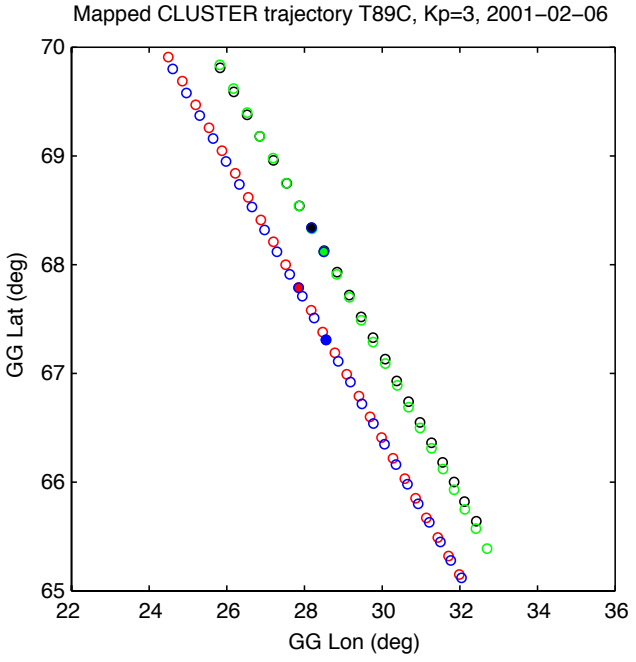

Fig. 1. Ground projection of C1 (black), C2 (red), C3 (green) and C4 (blue) trajectory on 6 February 2001 23:14–23:40 UT, with 1-min resolution. Solid dots show instantaneous position at 23:28 UT.

3 Observations

During the poleward motion over the northern auroral oval, Cluster s/c crossed two auroral arcs. The first arc had been visible to the ground all-sky cameras well before the Cluster arrival and in the following discussion, we will refer to it as the equatorward arc. Spacecraft C1, C2 and C4 traversed the equatorward arc (C3 was not operational during the event discussed in this paper). During the crossing of the equatorward arc, a pseudo-breakup occurred, and 8 min after that, a new arc started to form poleward of the equatorward arc, which will be referred to as the poleward arc. Spacecraft C1, which was the first one in the "string of pearls" configuration of Cluster, never caught this developing arc, but the following s/c C2 and C4 did. We will discuss these arcs separately in the following sections.

3.1 Equatorward arc

3.1.1 Ground optical and magnetic observations

A faint arc, which we refer to as the equatorward arc, is observed to drift equatorward from 23:09 UT onwards by the Sodankylä (SOD) all-sky camera. At 23:24 UT the arc is located in the zenith of SOD and the drift speed is about 180 m s^{-1}. The arc location, together with the mapped locations of the three Cluster s/c (C1 is black, C2 red and C4 blue), are shown in Fig. 2. The observations were made during conditions of a bright moon, which is visible in the figure.

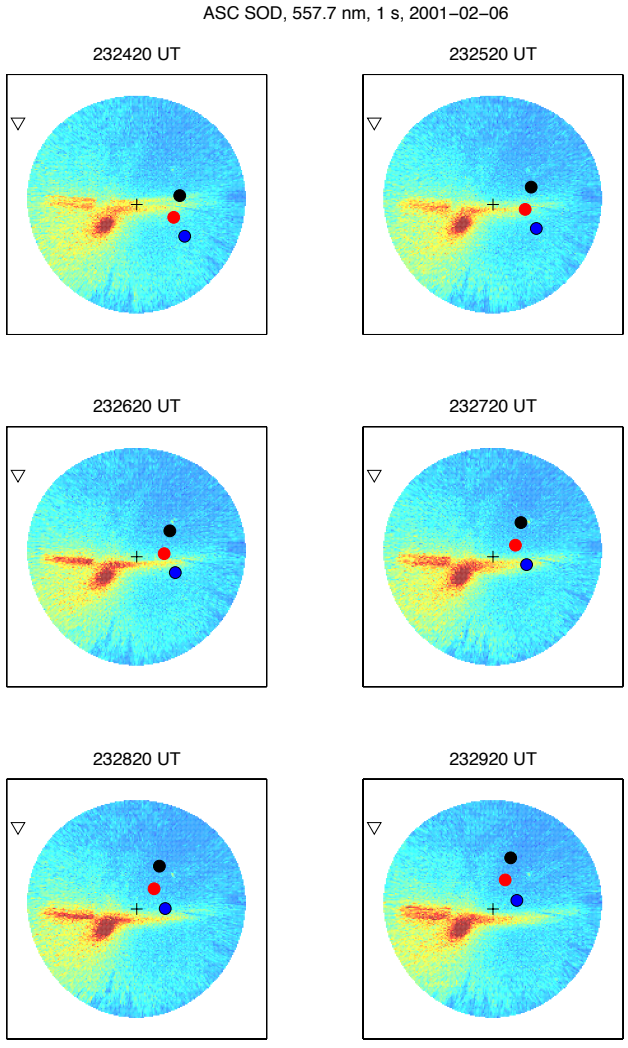

Fig. 2. Ground projection of the three operative Cluster s/c mapped according to T89c model, K_p=3 and the equatorward auroral arc measured by the SOD all-sky camera at 557.7 nm. Color coding for intensity (in arbitrary units) is used and the field of view of 140° at an altitude of 100 km is shown. The moon is visible in the direction of the arc and the triangle shows the location of EISCAT.

The arc terminates in the field of view (f-o-v) of the SOD ASC, just east of Cluster footpoints.

At 23:24 UT a burst of magnetic PiB pulsations (up to about 1 Hz) occurs at SOD and at a sub-auroral station, Nurmijärvi (NUR) (data not shown). NUR also records an onset of lower frequency Pi2 pulsations at about 23:24:40 UT, which have been used to time an onset of a substorm or a pseudo-breakup. We identify the 23:24:00–23:24:40 UT time interval as an onset of a pseudo-breakup. The SOD ASC shows that a clear intensification in the arc, though mainly west of Cluster s/c, starts at about 23:25:40 UT. However, in the longitude where all the Cluster s/c cross the arc, the intensity variations are small until 23:30 UT. The equatorward drift of the arc stops at about 23:28:20 UT and then the arc is almost stationary, with a small velocity poleward.

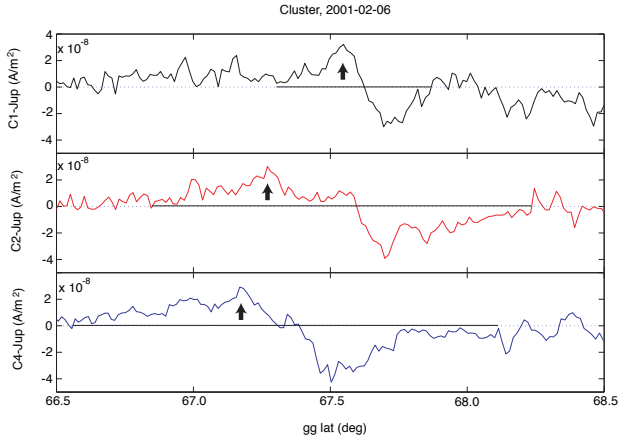

Fig. 3. FAC densities for C1, C2 and C4 as a function of geographic latitude, positive values mean upward current from the ionosphere. Arrows show the location of the maximum upward FAC and solid horisontal lines indicate the estimated widths of the current sheets. The times corresponding to arrows from top to bottom are: 23:24:10 UT, 23:25:25 UT and 23:27:20 UT.

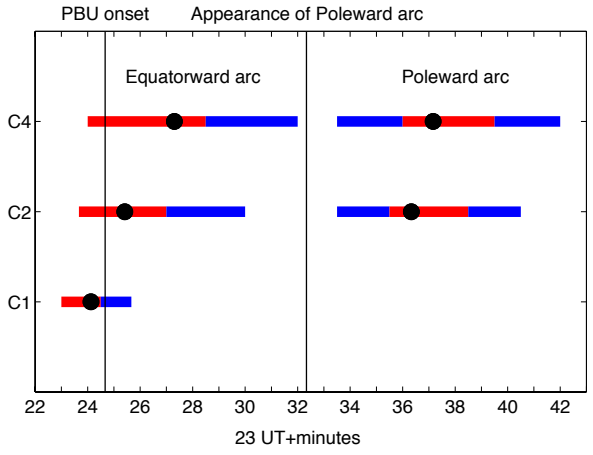

Fig. 4. Timeline of the C1, C2 and C4 crossings of the two arcs. Red (blue) horisontal bars denote upward (downward) FAC regions. Black dots denote times of maximum upward FACs. In addition, vertical lines show pseudo-breakup (PBU) onset time and the time when the poleward arc starts to form.

3.1.2 Cluster observations of field-aligned currents

Figure 3 shows the calculated FACs for the three s/c as a function of ground geographic latitude. The mapping has been made using the T89c K_p=3 model and the FAC density values associated with arcs have been corrected by arc motions, assuming that the arc and the associated current system move together. The corrected FAC density j_z^{arc} is calculated from the uncorrected FAC density j_z^{obs} by $j_z^{arc}=v_{sat}/(v_{sat}+v_{arc})\cdot j_z^{obs}$, with the plus sign in the denominator corresponding to the arc velocity being towards the satellite. During 23:23:20–23:28:20 UT the arc drifts with a velocity of 180 m s^{-1} southward and 23:28:20–23:29:40 UT at 80 m s^{-1} northward. Taking into account the satellite velocity of about 370 m s^{-1} northward in the ionosphere, the correction factors of FACs are 0.7 and 1.3 for the time periods in question. The magnitudes of FACs correspond to the measurement altitude and the values must be multiplied by about a factor of 110, the ratio between the magnetic field in the ionosphere and the measurement altitude, to obtain the current densities in the ionosphere. Figure 3 shows clearly the equatorward motion of the maximum in the upward current sheet, corresponding to the equatorward motion of the visual arc. The maximum intensity of the upward current stays at a very constant value of 3 μA m^{-2} (value mapped to the ionosphere) during all s/c passages, in accordance with the measurements by SOD ASC at the longitude of Cluster s/c, which indicate very small intensity variations in the arc. When the locations of the intensity maxima of the visual arc and the maxima of the upward FACs at the s/c are compared, they are colocated within 0.1° of latitude. The region of downward FAC is located just poleward of the upward FAC and for the downward FAC, the maximum current density value increases from 3 to 4 μA m^{-2} from C1 to C2 and C4.

Even though the current density values don't change much during the studied time interval, the width and the shape of the FAC system changes. Figure 4 shows the timeline of the Cluster crossing of the equatorward arc. The major change in the FAC system of the arc occurs between s/c C1 and C2 crossings of the arc. During the C1 crossing, the gradient between the up- and downward FAC is steep and the widths of the current sheets are comparable, about 30 km. During s/c C2 crossing, the widths of upward and downward FACs have grown to about 80 and 70 km, respectively, and only a small additional widening, to about 90 and 80 km, takes place when C4 crosses the arc. The temporal separation between the crossings of the maximum upward FAC is 80 s between C1 and C2 and 120 s between C2 and C4. If the FAC reversal is considered, then the temporal separations between C1 and C2 are 150 s and between C2 and C4 80 s.

The current densities integrated over the upward and downward FACs change from 50 and −50 mA/m at C1, respectively, to 100 and −115 mA/m at C2 and further to 120 and −130 mA/m at C4. The currents are rather well balanced, taking into account the uncertainties of calculations, for example, in defining the outer boundaries of the current sheets.

So, because of this widening, the total amount of current flowing in the arc current system doubles between the C1 and C2 crossings of the arc. The reason for the intensification of the FACs is the pseudo-breakup occuring at 23:24:40 UT (shown by a vertical line in Fig. 4). However, C1 leaves the downward FAC region of the arc at 23:25:40 UT, while it is still narrow, so the change in the current system doesn't take place immediately after the onset of a pseudo-breakup, but within 1–2 min.

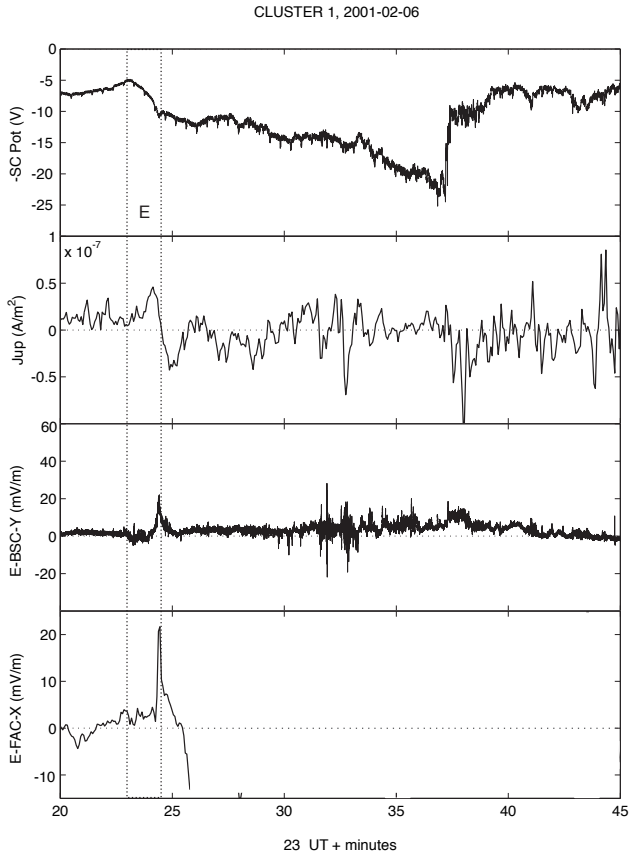

Fig. 5. Cluster 1 EFW anf FGM measurements. Panels from top to bottom: Negative of the s/c potential, FAC density (positive away from the ionosphere), BSC-Y component of the high-resolution electric field (every 10th point shown) and FAC-X component of the DC electric field. The equatorward (poleward) arc are denoted by E (P).

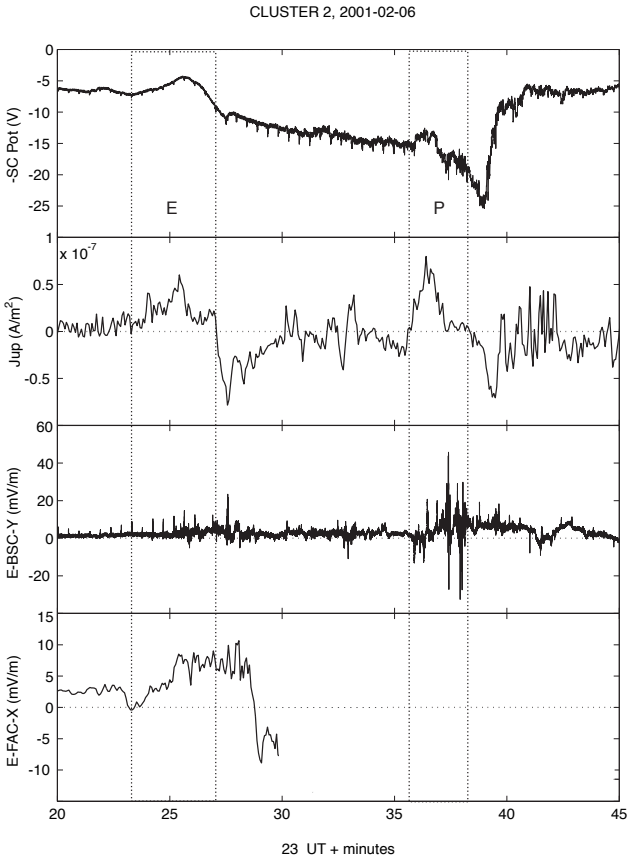

Fig. 6. As Fig. 5, but for C2.

3.1.3 Cluster electric field and potential observations

Figures 5, 6 and 7 show an overview of EFW and FGM measurements by C1, C2 and C4, respectively, from the whole time of interest. The crossing of the upward FAC sheet of the equatorward arc is denoted by dashed lines and marked by E. The top panel shows the negative of the spacecraft potential with respect to the probe potential, which is biased to a value close to the ambient plasma potential. The s/c potential is a function of electron density (and to a lesser extent also of the temperature), so that in dilute plasma the spacecraft potential increases and vice versa (Pedersen et al., 2001). According to the spacecraft potential, the arc is located at the equatorward boundary of a large-scale density cavity. The second panel shows the calculated FAC from the FGM measurement for comparison (the values are not corrected to take into account arc motions, since this cannot be done for the whole time interval). The third panel, showing the high-resolution electric field, will be discussed in the next section. The bottom panel shows the DC electric field in the north-south direction (positive southward), calculated up to the point where the magnetic field is 10° from the spin plane.

All three s/c measure a southward electric field in the region of the FACs associated with the arc. At all s/c, there is indication of the electric field turning northward at the poleward part of the downward FAC region, forming a divergent structure. It is unclear as to how the electric field maps to the ionosphere. In case of a quasi-static parallel potential difference with convergent or divergent perpendicular electric fields, the integrated perpendicular electric field along the s/c path corresponds to the parallel potential difference below the satellite. It has been shown in several cases that the potential drop obtained by integrating the convergent electric field along the s/c path is in accordance with the energy of upflowing ions or the widening of the electron loss cones observed at satellites above the auroral acceleration region (Temerin et al., 1981; Redsun et al., 1985; Marklund, 1993; McFadden et al., 1999). Vaivads et al. (2003) showed that the quasi-static U-shaped potential structure extended up to a geocentric distance of 4.7 R_E and the potential drop remained as 3–4 keV during the few minutes of the Cluster s/c 2–4 passage. Also, in downward current regions the diverging electric field produces integrated potentials which match the energy of upward accelerated electron beams, as shown by Carlson et al. (1998b), Ergun et al. (1998) and Marklund et al. (2001). Observations by Marklund et al. (2001) were made at geocentric distances of 4.4 R_E with Cluster, as in this event. However, without particle data, no clear conclusions can be drawn as

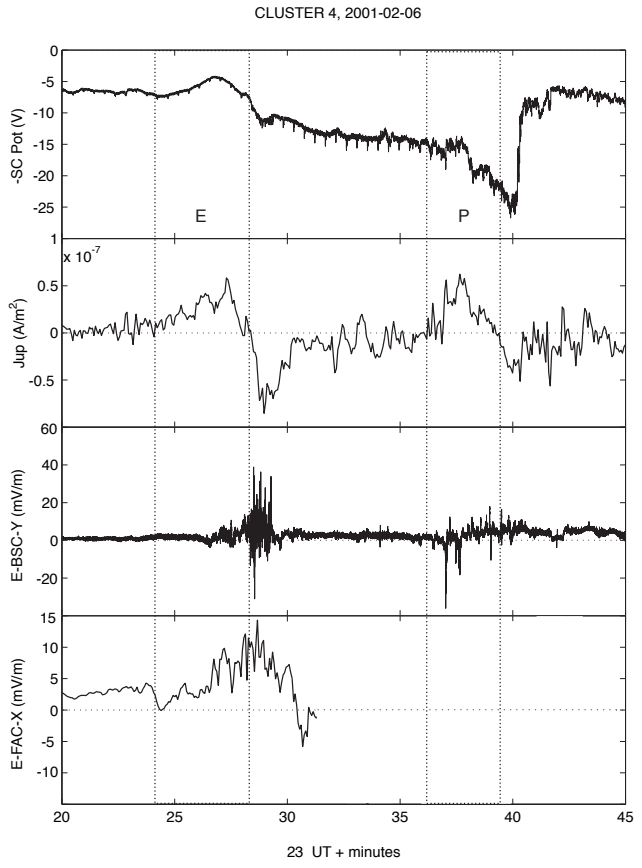

Fig. 7. As Fig. 5, but for C4.

to whether the observed diverging electric field maps to the ionosphere or not.

The southward electric field direction is in accordance with the observed FAC directions: the current circuit consists of a downward current sheet on the poleward side of the arc, an ionospheric southward Pedersen current and an upward current sheet from the arc. This kind of a current circuit is typical of morning sector arcs. There is an intense spike in the southward electric field close to the sharp current reversal region at C1. If it is an electrostatic structure and maps down to the ionosphere, it could correspond to the enhanced electric field at the edge of an arc within the downward FAC region, sometimes observed in the ionosphere (Opgenoorth et al., 1990; Aikio et al., 1993, 2002).

3.1.4 Cluster observations of electric field fluctuations

The third panel of Figs. 5, 6 and 7 shows the measured high-resolution electric field in the BSC-coordinate system. All Cluster s/c measure a small enhancement (amplitude less than 5 mV m^{-1}) in electric field fluctuations in the region comprising the up- and downward FAC pair of the arc (at C1 the DC component is also clearly visible). Only C4 measures intense, up to 40 mV m^{-1}, broad-band electric fluctuations within the downward current region during 23:28:20–23:29:30 UT. The frequency goes up at least to 150 Hz, though most of the power is below 50 Hz (plot not shown). At that time C2 is also within the downward FAC region, but in the poleward part of it, and sees no intense fluctuations (Fig. 4).

So, broad-band electric fluctuations were spatially confined to the most intense part of the downward FAC sheet, located next to the FAC reversal region. They were also limited in time: C2, which crossed the maximum downward FAC about 90 s earlier than C4, didn't see them. The external conditions in terms of current density, electric field and plasma potential were similar during the C2 and C4 crossings of the downward FAC. Unfortunately, no particle measurements exist from that time. Ground optical observations showed that at about 23:28:20 UT the equatorward drift of arc stops; so the burst of broad-band waves occurs just after that.

3.2 Poleward arc

3.2.1 Ground optical and magnetic observations

At about 23:32:20 UT a new auroral patch starts to form just equatorward of the zenith of ABK (located about 1° to the north and 8° to the west of SOD in geographic coordinates), intensifies and expands slowly eastward and poleward. At 23:35:20 UT the patch has developed into an arc at ABK zenith, which we shall refer to as the poleward arc. Figure 8 shows selected frames of ABK all-sky camera frames together with mapped locations of the three Cluster s/c. After 23:30 UT the mapping with K_p=3 in the T89c model put all s/c too much poleward, but a change to K_p=5 produces good agreement with ground observations. This change can be justified by the effects of the pseudo-breakup on the configuration of the magnetic field. The 23:36:20 UT frame shows that a fold exists in the eastern part of the arc. At the same time s/c C2 is at the latitude of the bright arc, though from the figure it seems that C2 would not be located in the most intense part of the arc. When looking at the figure, one should remember that false color coding of intensity (not calibrated to physical units) is used, there are uncertainties in the mapping of ASC images at the lowest elevations and also uncertainties in mapping the satellites to the ground. Even occasional small clouds can hide a part of the ASC image. Spacecraft C4 is clearly within the bright fold at 23:37:20–23:38:20 UT and after that the fold has travelled eastward outside the ASC field of view.

In ground magnetograms the 23:00–24:00 UT period is only slightly disturbed, maximum horizontal negative deflections are about 140 nT in the region equatorward of the equatorward arc, indicating WEJ flow in that area (Amm et al., 2003). So, in the Scandinavian sector the event starting at 23:24 UT appears as a pseudo-breakup, as discussed already in Sect. 3.1.1.

3.2.2 Cluster observations of field-aligned currents

Figure 9 shows the calculated FACs for the three s/c as a function of ground geographic latitude after crossing the

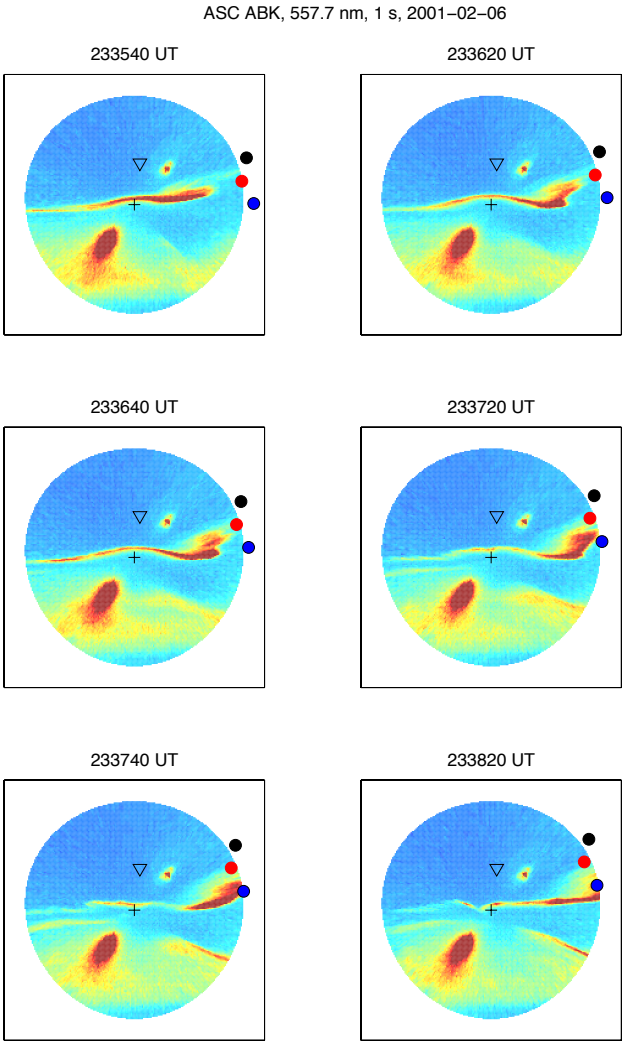

Fig. 8. As Fig. 2, but for ABK and the poleward arc.

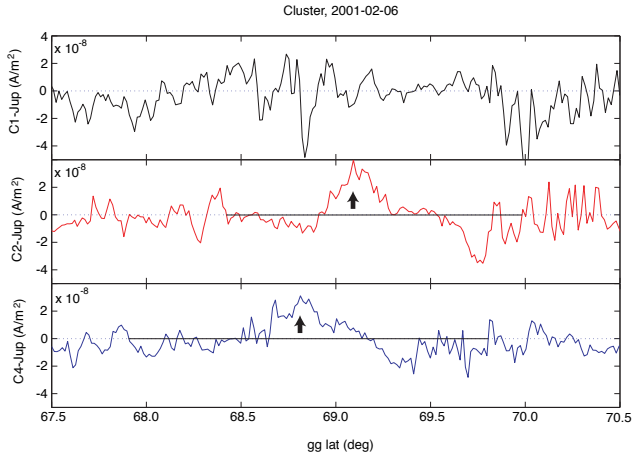

Fig. 9. As Fig. 3, but now for the poleward arc and using T89c K_p=5. The times corresponding to arrows from top to bottom are: 23:36:30 UT and 23:37:40 UT.

equatorward arc. Again, the FAC values have been corrected by arc motions, as explained in Sect. 3.1.2.

C1 measures alternating up- and downward currents between 23:31 and 23:35 UT (Fig. 5), which are associated with subvisual arcs. According to the ABK ASC measurement at the longitude of 25°, very faint arcs are located during that time at 68.7–68.9° latitude range, in the same region where C1 measures the most intense FACs.

C2 enters an upward current region at 23:35:40 UT and C4 70 s later (Figs. 6 and 7). Since the arc is very faint before 23:34:20, its velocity has not been determined. This arc obviously drifts poleward, which would intensify the FAC values measured by C1. During 23:35:40–23:37:40 UT the maximum of the intensity of the arc drifts equatorward with a velocity of 440 m s^{-1} at the longitude of 25°, as measured by the ASC. This motion can also be seen in the Cluster FAC data. This results in a correction factor of 0.5 to the calculated FAC intensities.

The region of the optical arc with the fold corresponds to an upward current, which has a maximum density of 4 μA m^{-2} at C2 and 3 μA m^{-2} at C4 (values mapped to the ionosphere). On the equatorward side of the arc there is a weak downward FAC region and on the poleward side an intense downward FAC region. The maximum densities of downward FACs are about 1 μA m^{-2} on the equatorward side and 4 and 3 μA m^{-2} on the poleward side for C2 and C4, respectively. The maximum upward FAC was measured between 23:36 and 23:37 UT by C2 and 23:37 and 23:38 UT by C4, and the ASC data show that it is measured from the region of the fold by both satellites. However, after 23:38:40 UT the fold has moved east of the Cluster longitude, but the arc remains bright until 23:39:40 UT, after which the intensity starts to decrease. The timeline of the Cluster crossing of the poleward arc is shown in Fig. 4.

The widths of the down-up-down FAC regions at the ionospheric level are estimated as 50–70–50 km at C2 and 70–70–70 km at C4 (Fig. 9, solid horizontal lines). However, the currents integrated along latitude remain the same, as 30–95–70 mA/m (within an uncertainty of 5 mA/m) during both satellite passes. The widths of the downward FAC regions are not very clearly defined but the width of the upward FAC can be determined rather accurately.

3.2.3 EISCAT observations

Between 23:35 and 23:37 UT the EISCAT radar observes a formation of a deep electron density cavity. The electron densities decrease at all altitudes between 100 and 600 km, though most clearly in the lower F- and E-region, and the ion temperature increases by a factor of about 3, indicating ion frictional heating by a very intense electric field (Fig. 10). During the next minute, the cavity still exists, but the electron densities start to increase and the ion temperature to decrease. The north-south component of electric field is measured by the coherent STARE radar and at the latitude of EISCAT an intense southward electric field starts to develop at 23:35 UT (Fig. 4 of Amm et al., 2003), in agreement with EISCAT

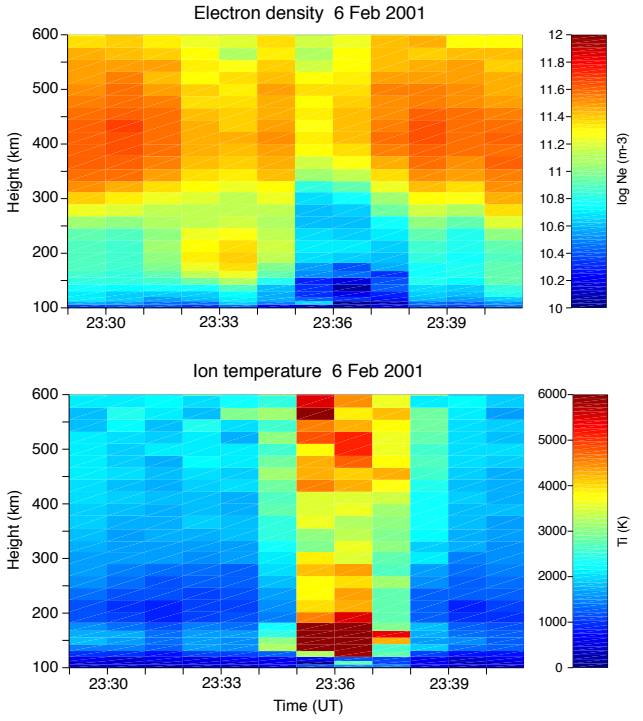

Fig. 10. EISCAT measurement from the downward FAC region poleward of the arc. Top panel shows electron densities and bottom panel ion temperature.

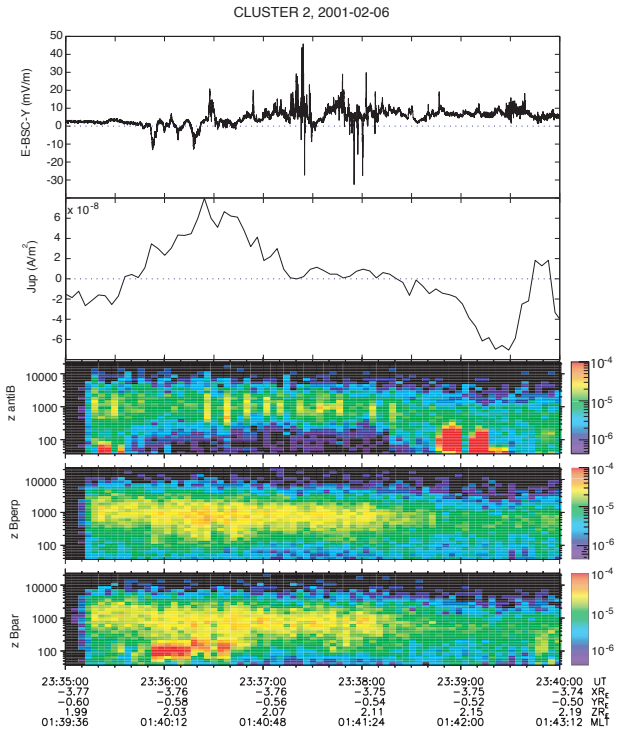

Fig. 11. Electron fluxes together with FACs and electric fluctuations measured by C2. From top to bottom: high-resolution electric field from the EFW, FAC (positive values correspond to current away from the ionosphere) from the FGM, and electron fluxes in the anti-parallel, perpendicular and parallel to B directions from the PEACE HEEA instrument in units of erg cm^{-2} str^{-1} s^{-1} eV^{-1} (calibration version 5).

observations. The formation of the density cavity coincides with the appearance of the bright arc at the ABK zenith and the cavity exists approximately as long as the bright arc at the longitude of EISCAT (shown as a triangle in Fig. 10), which is located poleward of the arc at a distance of about 80 km from the center of the arc during this time. Obviously EISCAT is located in the region of the downward FAC of the arc at this time, but probably close to the poleward edge of this region, as deduced from the estimated widths of FACs by Cluster.

3.2.4 Cluster observations of particles

The PEACE instrument was switched on at about 2335:40 UT, after the preventive switch-off period in the radiation belts. Figure 11 shows the high-energy detector HEEA measurements of electron fluxes for C2 from 36 eV to 23 keV in the three bottom panels; in the two top panels the FAC and electric field fluctuations are shown for reference. The three bottom panels from top to bottom are electron fluxes in the anti-parallel (upward), perpendicular and parallel (downward) to B directions, measured within an angle of 15°. All the panels show an electron population of a mean energy of about 1 keV, which is probably of plasma sheet origin. The flux densities and mean energy of this population decrease after 23:39 UT, when C2 leaves the large-scale density cavity.

Within the region of the upward FAC from the arc, intense fluxes of downgoing <200 eV electrons (bottom panel) are observed during the most intense upward FAC, 23:35:50–23:36:40 UT. When the detector is looking upward, plasma is depleted at energies lower than 200 eV. This indicates a local acceleration of the whole electron population in the downward direction.

The upward moving electrons (top panel of PEACE data) show two enhancements of flux occurring at low energies. The first one with $\leq$100 eV electrons corresponds to a region of a weak downward FAC on the equatorward side of the arc, which lasts until 23:35:45 UT, according to the magnetometer measurement. The second one with intense fluxes $\leq$300 eV upgoing electrons occurs during 23:38:50–23:39:40 UT and corresponds to the intense downward FAC region on the poleward side of the arc. The upgoing electron beams have a broad energy range and they are more collimated than those in the upward FAC region (high resolution data, not shown). The electrons are accelerated below Cluster and the narrow width indicates that they are cold electrons accelerated parallel to magnetic field lines.

PEACE was turned on later at C4, at 23:37:21 UT while C4 was within the upward FAC region. The basic features observed by C2 are also observed at C4. Figure 12, bottom panel, shows again an intense flux of downgiong low-energy (<200 eV) electrons from the upward FAC region. In this case, the maximum energy of the beams decrease from

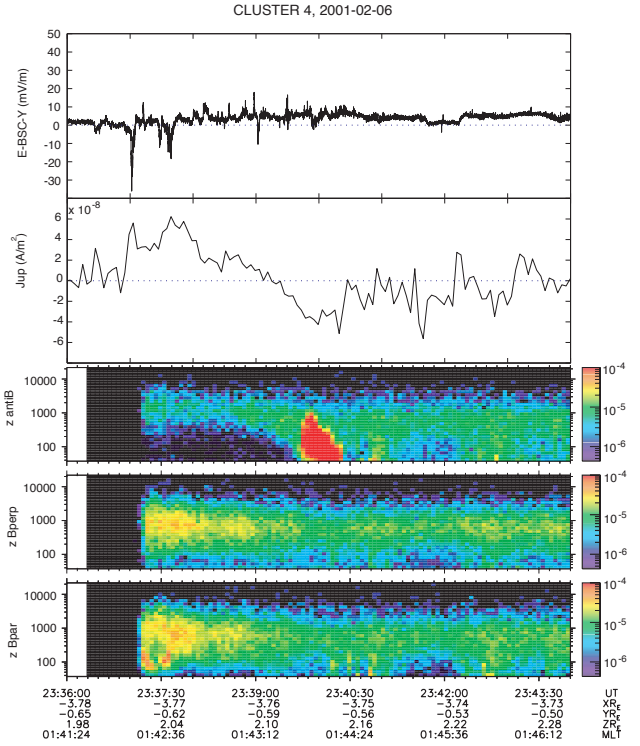

Fig. 12. As Fig. 11, but for C4.

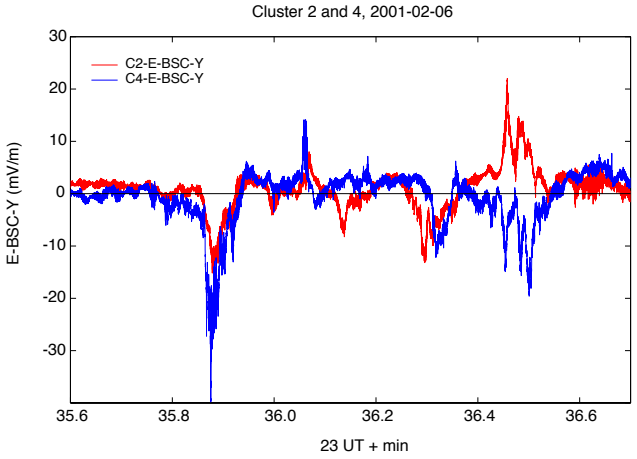

Fig. 13. The high-resolution electric field BSC Y-component from the EFW measurement from C2 (blue) and C4 (red), C4 data shifted by 69 s earlier in time.

200 to 100 eV in the middle of the event. The most pronounced feature is, however, the intense flux of upgoing electrons measured from the region of the downward FAC during 23:39:40–23:40:30 UT. Now energies reach up to 1 keV and the maximum energy along latitude resembles an asymmetric inverted-V structure.

3.2.5 Cluster electric field and potential observations

The probe potentials (top panels in Figs. 5, 6 and 7) indicate that all the satellites are still located inside the large-scale density cavity, which was bounded from the equatorward side by the equatorward arc. Lowest densities are found on the poleward side of the poleward arc and then densities rise very rapidly, forming a steep poleward boundary of the density cavity. All satellites observe the density cavity, also C1 even though at that time there is no arc close to the poleward boundary of the cavity. So, the cavity is a more long-lived structure than the arcs.

During the time of interest the magnetic field lies within 10° from the spin plane, so that the FAC coordinate system cannot be used for calculating the electric field. Figures 11 and 12, second panel from the top, show the Y-component of the high-resolution electric field in the BSC coordinate system (Sect. 2), where the most intense variations are seen. The Y-component may contain contributions from both the NS and EW components of the FAC coordinate system and the total magnitude of the electric field perpendicular to B cannot be derived. Two different kinds of fluctuations on the electric field can be seen: the intense low-frequency variations measured by C2 between 23:35:40 and 23:36:40 UT in the upward FAC region and the even more intense broad-band fluctuations between 23:37:15 and 23:38:15 UT in the downward FAC region (Fig. 11).

The first type, the low-frequency electric field fluctuations at C2, comprise the equatorward half of the upward FAC region and also C4 measures similar type of fluctuations in the same location with respect to the FAC during 23:36:50–23:37:50 UT (Fig. 12). When C4 data are shifted forward in time by 69 s, corresponding to the time difference between C2 and C4 crossings of the arcs, it can be seen that the structures are almost similar at the two s/c (Fig. 13). The most significant differences are the enhancement of the first spike from 15 to 40 mV m^{-1} and the change in sign of the last spike. The spatial size in the perpendicular to B direction of the individual spikes varies from about 2 to 24 km at the measurement altitude and a typical value is from 2.5 to 5 km. If mapped to the ionosphere, these values must be divided by the geometric factor of about 12. The separation of C2 and C4 in the east-west direction in the plane perpendicular to B is about 130 km for T96. The spatial scale of the structures is clearly smaller than this separation and hence we suggest that the variations occur in the NS direction and are elongated along the arc in the EW and field-aligned directions. The separation of C2 and C4 in the field-aligned direction is about 250 km.

The second type, the intense broad-band electric field fluctuations (amplitudes up to 50 mV/m) at C2 appear between 23:37:15 and 23:38:15 UT as two bursts. At that time the satellite is located between the intense up- downward FAC regions, within a very weak upward FAC with no up- or downgoing low-energy electron beams. At the same time C4 is in the intense upward FAC region and doesn't measure broad-band fluctuations. When C4 enters the weak upward FAC region 70 s later, broad-band fluctuations don't appear anymore. Again, the broad-band electric fluctuations are limited in time and space.

Also, C1 observes broad-band electric field fluctuations (Fig. 5) and they are confined to the downward FAC regions of the subvisual arcs 23:31:30–23:33:00 UT, and don't exist in the upward FAC regions.

The electric field fluctuations are discussed more in Sect. 4.2.

4 Summary and discussion

4.1 Temporal evolution of the arcs

Here we briefly summarise the temporal evolution of the two arcs in terms of field-aligned currents and ground-based observations. The equatorward arc is associated with a current system consisting of an upward FAC from the arc and a downward FAC poleward of it, obviously connected by an equatorward Pedersen current in the ionosphere, typical of morning sector arcs. The total FAC doubles between the C1 and C2 crossings of the arc, separated by 80–150 s. The increase is due to a widening of the FAC sheets, not an increase in current densities, and it occurs in association with an onset of a pseudo-breakup. It takes 1–2 min for the current systems to evolve after the onset of Pi2 pulsations, which are commonly used to time the onsets (Rostoker et al., 1980). The gradual development of the current systems may indicate that it takes several bounces of Alfvén waves between the magnetosphere and the ionosphere to set up the new current system after changes in the magnetosphere. Optically, the arc starts to intensify at the same time as the FACs start to widen. The equatorward drift of the arc stops and a fold in the arc appears drifting from the west about 4 min after the onset of Pi2 pulsations, so the onset of the pseudo-breakup occurs obviously closer to the magnetic midnight and expands towards Scandinavia, which is in the post-midnight sector. About 8 min after the onset, the poleward arc starts to form.

Two Cluster s/c (C2 and C4) cross the poleward arc and especially the fold in it. Since optical data show that the fold moves slowly eastward, some of the changes between C2 and C4 might be of spatial, not temporal origin. However, the width (70 km) and the density of the upward FAC are almost similar at the two s/c, which indicate that both of them cross the fold. In addition, the electric field structures in the upward FAC are almost similar at C2 and C4. For the poleward arc, the return current (downward FAC) regions are located on both sides of the arc, but the poleward return current is wider and more intense. EISCAT radar observations show formation of an electron density cavity in the ionospheric E- and F-regions, poleward of the arc, during the time the arc is bright at the meridian of EISCAT. The density cavity thus occurs in the region of the downward FAC and PEACE data indicates that upflowing ionospheric electrons carry this current. As the density cavity in the ionosphere forms, the ionospheric Pedersen conductance decreases and the return current region forms a growing load for the current circuit. In order to maintain the horizontal part of the current system, the horizontal electric field has to increase, as happens according to the EISCAT and STARE observations. Also, the evacuation of ionospheric electrons carrying the field-aligned return current implies that, in order to maintain a sufficient return current, either the energy of the electrons must be increased or the current region should be widened. Cluster observations show that both of the processes occur. PEACE data indicate that the ionospheric cold electrons are accelerated below 4.4 R_E, first to energies up to 200 eV and 70 s later to 1000 eV. Also, the width of the return current increases from about 50 to 70 km while the maximum current density decreases and as a result, the total amount of return current remains constant. These observations are in agreement with Cluster observations of morning sector aurora within the same altitude range by Marklund et al. (2001), who observed the following. A diverging electric field was colocated with upward electron beams and the corresponding electric potential agreed roughly with the energy of the electron beams. The potential grew in magnitude and width for about 200 s, accompanied by a widening of the downward FAC sheet, with the total current remaining constant, after which it faded away. Observational evidence of cavities at the poleward edge of the auroral oval are shown by Doe et al. (1993) and within the return current region by Aikio et al. (2002). The basic physical reason for the formation of the cavity is that the downward FAC is carried by upward moving ionospheric electrons, whereas the horisontal Pedersen current is carried by ions in the E- and lower F-region and in order to maintain plasma neutrality, a net outflow of charge carriers occurs in the current closure region. Simulations by Doe et al. (1995) showed that a current density of 0.2 μA m^{-2} created a cavity in 30 s and a model with different boundary conditions by Karlsson and Marklund (1998) showed formation of a cavity in a time scale of seconds for a current density of 10 μA m^{-2}.

In summary, we observe two different temporal evolutions of arcs: (1) As a response to a pseudo-breakup onset, both the up- and downward FAC sheets associated with the equatorward arc widen and the total amount of FAC doubles in a time scale of 1–2 min. (2) In the poleward arc, a density cavity forms in the ionosphere in the return (downward) current region. As a result of ionospheric feedback, strongly enhanced ionospheric southward electric field develops in the region of decreased Pedersen conductance. Furthermore, the acceleration potential of ionospheric electrons, carrying the return current, increases from 200 to 1000 eV in 70 s and the return current region widens, in order to supply a constant amount of return current to the arc current circuit.

4.2 Electric field fluctuations

It is well known that broad-band low-frequency (from DC to the lower hybrid cut-off frequency) waves, generally referred to as broad-band ULF/ELF (BBELF) waves or turbulence, exist on auroral field lines and in the cusp region (e.g. Gurnett et al., 1984; Block et al., 1987; Lundin and Eliasson, 1991; Aikio et al., 1995, 1996; Chaston et al., 1999; Angelopoulos et al., 2001). The waves in the auroral

zone from the upper part of the ionosphere to altitudes over 20 000 km have a magnetic component that decreases with altitude and frequency faster than the electric field component, so they are primarily electrostatic at high altitudes. The nature of these waves is still under discussion. Angelopoulos et al. (2001) analysed Polar s/c data and concluded that the observed broad-band waves were due to homogenous, low-frequency, broad k-spectrum spatial structures Doppler-shifted to the observed frequency range owing to spacecraft motion. Stasiewicz et al. (2000a, b) concluded that broad-band waves below 500 Hz represented mainly spatial turbulence of dispersive Alfvén waves. The term dispersive Alfvén wave (DAW) was adopted to include both the inertial and kinetic effects which result in a field-aligned electric field in the wave. Wahlund et al. (2003) studied Cluster observations of broad-band waves in association with auroral activity at distances of 4–5 R_E and suggested that they were DAWs propagating down the magnetic field lines.

In this study, the observed BBELF waves at a geocentric distance of about 4.4 R_E were mainly electrostatic, though at some instances there was indication of simultaneous magnetic fluctuations (high resolution magnetic data, not shown). The possibility to use three closely spaced satellites revealed that BBELF waves were highly localised in space and time, so visual auroral arcs are not all the time associated with broad-band electric field fluctuations at high altitudes. The BBELF waves were observed in the downward FAC region of the equatorward arc by C4, in the downward FAC regions of subvisual arcs by C1, but in the very weak upward FAC region of the poleward arc by C2. So, it is clear that broad-band waves are associated with aurora, though not necessarily the visual arc but also the return current region adjacent to the arc.

It is beyond the scope of this paper to try to identify the generation mechanism of the observed BBELF waves. However, we can note that the conditions in terms of DC electric field, FAC density and plasma density at the measurement altitude were not different at s/c observing/not observing broad-band waves. For the equatorward arc, no particle measurements existed, and for the poleward arc, only electron data was available. It is well known that BBELF waves are typically associated with ion heating (André et al., 1998; Lynch et al., 2002).

A somewhat different kind of low-frequency electric field fluctuations was observed in the upward FAC of the poleward arc. The fluctuations did not contain as high frequencies as the BBELF waves discussed above. In addition, comparison of C2 and C4 data showed that they retained their structuring during at least 70 s (the temporal separation of the s/c). Suprathermal (up to 200 eV), locally accelerated, downgoing electron beams were located within the same region.

Plenty of experimental evidence exists for colocation of bursts of suprathermal electrons and DAW at low altitudes (Boehm et al., 1990; McFadden et al., 1999; Ivchenko et al., 1999; Lynch et al., 1999; Andersson et al., 2002). Typical perpendicular wavelengths of DAW have been observed as 250–500 m and larger by Andersson et al. (2002) and 40 m–10 km by Stasiewicz et al. (2000a).

In this study, the electron density at the measurement altitude can be deduced from the s/c potential of 10 to 15 V, which corresponds to an electron density of about 1 cm^{-3} (Pedersen et al., 2001), resulting in an electron skin depth λ_e of 5 km. Electron inertial effects start to rise when $k_\perp \lambda_e \geq 1$, i.e. when $\lambda_\perp \leq 2\pi\lambda_e$ (e.g. Stasiewicz et al., 2000a, b), in this case corresponding to a perpendicular wavelength of about 30 km. Since the width of most of the structures was clearly smaller than that (2–24 km at the measurement altitude), they could correspond to dispersive Alfvén waves with a parallel electric field at the wave front.

Electron acceleration by DAWs has been studied in several papers. In the time-dependent DAW, accelerated electrons occur in transient bursts at the leading edge of an Alfvén wave pulse (e.g. Kletzing, 1994). Under some circumstances, dispersive Alfvén waves can produce quasi-stationary structures (e.g. Hui and Seyler, 1992; Knudsen, 1996; Streltsov and Lotko, 1999). It is clear that since the observed field-aligned electrons are of low energy (200 eV), their energy is not enough to produce the visible auroral arc observed at the wavelength of 557.7 nm (and only weakly at 630 nm), but they must be further energised below the s/c. This can be accomplished by the dispersive Alfvén wave, which can pick up cold electrons and accelerate them all the way down to the upper ionosphere or by a quasi-static upward pointing electric field below the s/c.

5 Conclusions

We have studied the temporal evolution of two auroral arcs at a radial distance of 4.4 R_E by the Cluster s/c and in the ionosphere by optical, magnetic and EISCAT radar observations. The arcs were located close to the equatorward and poleward edge of a large-scale density cavity, respectively. The EFW and FGM measurements exist from both of the arcs, but electron measurements by the PEACE instrument exist only from the poleward arc. The two arcs showed a different kind of temporal evolution. (1) As a response to a pseudo-breakup onset, the FAC sheets widened and the total amount of FAC doubled during 1–2 min in the equatorward arc. (2) In the poleward arc, the return (downward) current was carried by narrow electron beams of broad energy range, indicating ionospheric origin. EISCAT measurements showed that a density cavity formed in the ionosphere in the return current region. As the density cavity in the ionosphere formed, the ionospheric Pedersen conductance decreased and the return current region formed a growing load for the current circuit. In order to maintain the horizontal part of the current system, the horizontal electric field had to increase. Furthermore, the acceleration potential of ionospheric electrons, carrying the return current, increased and the return current region widened in order to supply a constant amount of return current. The energy increase of electrons was from

200 to 1000 eV in 70 s and the widening of the downward FAC region from about 50 to 70 km.

Evidence of local acceleration of the electron population by dispersive Alfvén waves was obtained in the upward FAC region of the poleward arc. However, the downward accelerated suprathermal electrons must be further energised below Cluster in order to be able to produce the observed visible aurora.

Broad-band low-frequency electric field (BBELF) waves with amplitudes up to 50 mV/m were observed in association with both arcs, in regions of downward or weakly upward FAC. The BBELF waves were highly localised in space and time, and could appear/disappear between two s/c passages of the same arc, which were separated by 60–90 s. So, visual auroral arcs are not all the time associated with broad-band intense electric field fluctuations at high altitudes, though commonly observed by satellites.

Acknowledgements. We thank R. Kuula for assistance in analysing EISCAT data and J. Jussila for processing the ASC data. We acknowledge K. Kauristie from FMI for providing us the all-sky camera data. The work by A. Aikio and O. Amm was supported by the Academy of Finland.

The Editor in Chief thanks two referees for their help in evaluating this paper.

References

Aikio, A. T., Opgenoorth, H. J., Persson, M. A. L., and Kaila, K. U.: Ground-based measurements of an arc-associated electric field, J. Atmos. Terr. Phys., 55, 797–808, 1993.

Aikio, A. T., Marklund, G. T., Woch, J., and Potemra, T. A.: Small scale structures in the high-altitude auroral electric field, Ann. Geophys., 13, 84–94, 1995.

Aikio, A. T., Blomberg, L. G., Marklund, G. T., and Yamauchi, M.: On the origin of the high-altitude electric field fluctuations, J. Geophys. Res., 101, 27 157–27 170, 1996.

Aikio, A. T., Lakkala, T., Kozlovsky, A., and Williams, P. J. S.: Current systems of stable drifting auroral arcs in the evening sector, J. Geophys. Res., 107, A12, SIA 3-1–SIA 3-14, doi:10.1029/2001JA009172, 2002.

Amm, O., Aikio, A., Bosqued, J.-M., Dunlop, M., Fazakerley, A., Janhunen, P., Kauristie, K., Taylor, M., Vontrat-Reberac, A., Mursula, K., and Andre, M.: Mesoscale structure of a morning sector ionospheric shear flow region determined by conjugate Cluster II and MIRACLE ground-based observations, Ann. Geophys., 21, 1737–1751, 2003.

Andersson, L., Wahlund, J.-E., Clemmons, J., Gustavsson, B., and Eliasson, L.: Electromagnetic waves and bursty electron acceleration: implications from Freja, Ann. Geophys., 20, 139–150, 2002.

André, M., Norqvist, P., Andersson, L., Eliasson, L., Eriksson, A. I., Blomberg, L., Erlandson, R. E., and Waldemark, J.: Ion energization mechanisms at 1700 km in the auroral region, J. Geophys. Res., 103, 4199–4222, 1998.

Angelopoulos, V., Mozer, F. S., Bonnel, J., Temerin, M., Somoza, M., Peterson, W. K., Collin, H. L., and Giles, B.: Wave power studies of cusp crossings wqith the Polar satellite, J. Geophys. Res., 106, 5987–6006, 2001.

Balogh, A., Dunlop, M. W., Cowley, S. W. H., et al.: The Cluster magnetic field investigation Space Sci. Rev., 79, 65–91, 1997.

Block, L. P., Fälthammar, C.-G., Lindqvist, P.-A., Marklund, G., Mozer, F. S., Pedersen, A., Potemra, T. A., and Zanetti, L. J.: Electric field measurements on Viking: First results, Geophys. Res. Lett., 14, 435–438, 1987.

Boehm, M. H., Carlson, C. W., McFadden, J. P., Clemmons, J. H., and Mozer, F. S.: High-resolution sounding rocket observations of large-amplitude Alfvén waves, J. Geophys. Res., 95, 12 157–12 171, 1990.

Carlson, C. W., McFadden, J. P., Ergun, R. E., et al.: FAST observations in the downward auroral current region: Energetic upgoing electron beams, parallel potential drops, and ion heating, Geophys. Res. Lett., 25, 2017–2020, 1998a.

Carlson, C. W., Pfaff, R. F., and Watzin, J. G.: The Fast Auroral SnapshoT (FAST) mission, Geophys. Res. Lett., 25, 2013–2016, 1998b.

Chaston, C. C., Carlson, C. W., Peria, W. J., Ergun, R. E., and McFadden, J. P.: FAST observations of inertial Alfvén waves in the dayside aurora, Geophys. Res. Lett., 26, 647–650, 1999.

Doe, R. A., Mendillo, M., Vickrey, J. F., Zanetti, L. J., and Eastes, R. W.: Observations of nightside auroral cavities, J. Geophys. Res., 98, 293–310, 1993.

Doe, R. A., Vickrey, J. F., and Mendillo, M.: Electrodynamic model for the formation of auroral ionospheric cavities, J. Geophys. Res., 100, 9683–9696, 1995.

Ergun, R. E., Carlsen, C. W., McFadden, J. P., et al.: FAST satellite observations of electric field structures in the auroral zone, Geophys. Res. Lett., 25, 2025–2028, 1998.

Gurnett, D. A., Huff, R. L., Menietti, J. D., Burch, J. L., Winningham, J. D., and Shawhan, S. D.: Correlated low-frequency electric and magnetic noise along the auroral field lines, J. Geophys. Res., 89, 8971–8985, 1984.

Gustafsson, G., Bostrom, R., Holback, B., et al.: The electric field and wave experiment for the Cluster mission, Space Sci. Rev., 79, 137–156, 1997.

Hui, C.-H. and Seyler, C. E.: Electron acceleration by Alfvén waves in the magnetosphere, J. Geophys. Res., 97, 3953–3963, 1992.

Ivchenko, N., Marklund, G., Lynch, K., Pietrowski, D., Torbet, R., Primdahl, F., and Ranta, A.: Quasiperiodic oscillations observed at the edge of an auroral arc by Auroral Turbulence 2, Geophys. Res. Lett., 26, 3365–3368, 1999.

Johnstone, A. D., Alsop, C., Burge, S., et al.: PEACE: a plasma electron and current experiment Space Sci. Rev., 79, 351–398, 1997.

Karlsson, T. and Marklund, G.: Simulations of effects of small-scale auroral current closure in the return current region, Phys. Space Plasmas 15, 401–407, 1998.

Kletzing, C. A.: Electron acceleration by kinetic Alfvén waves, J. Geophys. Res., 99, 11 095–11 103, 1994.

Knudsen, D. J.: Spatial modulation of electron energy and density by nonlinear stationary inertial Alfvén waves, J. Geophys. Res., 101, 10 761–10 772, 1996.

Lundin, R. and Eliasson, L.: Auroral energization processes, Ann. Geophys., 9, 202–223, 1991.

Lynch, K. A., Pietrowski, D., Torbet, R. B., Ivchenko, N., Marklund, G., and Primdahl, F.: Multiple-point electron measurements in a nightside auroral arc: Auroral Turbulence II particle observations, Geophys. Res. Lett., 26, 3361–3364, 1999.

Lynch, K. A., Bonnel, J. W., Carlson, C. W., and Preria, W. J.: Return current region aurora: $E_{\|}$, j_z, particle energization, and broad-band ELF wave activity, J. Geophys. Res., 107, A7, SMP

16-1–SMP 16-19, doi:10.1029/2001JA900134, 2002.
Marklund, G. T.: Viking Investigations of Auroral Electrodynamic Processes, J. Geophys. Res., 98, 1691–1704, 1993.
Marklund, G. T. and Karlsson, T.: Characteristics of the Auroral Acceleration in the Upward and Downward Current Regions, Phys. Chem. Earth (C), 26, 181–96, 2001.
Marklund, G., Blomberg, L., Fälthammar, C.-G., and Lindqvist, P.-A.: On intense diverging electric field associated with black aurora, Geophys. Res. Lett., 21, 1859–1862, 1994.
Marklund, G., Karlsson, T., and Clemmons, J.: On low-altitude particle acceleration and intense electric fields and their relationship to black aurora, J. Geophys. Res., 102, 17 509–17 522, 1997.
Marklund, G. T., Ivchenko, N., Karlsson, T., et al.: Temporal evolution of the electric field accelerating electrons away from the auroral iuonosphere, Nature, 414, 724–727, 2001.
McFadden, J. P., Carlson, C. W., and Ergun, R. E.: Microstructure of the auroral acceleration region as observed by FAST, J. Geophys. Res., 104, 14 453–14 480, 1999.
Mozer, F. S., Carlson, C. W., Hudson, M. K., Torbert, R. B., Parady, B., Yatteau, I., and Kelley, M. C.: Observations of paired electrostatic shocks in the polar magnetosphere, Phys. Rev. Lett., 38, 292–295, 1977.
Olsson, A. and Janhunen, P.: Some recent developments in understanding auroral electron acceleration processes, IEEE Transactions on Plasma Science, 31(6), 1178–1191, 2003.
Opgenoorth, H. J., Häggström, I., Williams, P. J. S., and Jones, G. O. L.: Regions of strongly enhanced perpendicular electric fields adjacent to auroral arcs, J. Atmos. Terr. Phys., 52, 449–458, 1990.
Pedersen, A., Decreau, P., Escoubet, C.-P., Gustafsson, G., Laakso, H., Lindqvist, P.-A., Lybekk, B., Mozer, F., and Vaivads, A.: Cluster four-point high time resolution information on electron densities, Ann. Geophys., 19, 1483–1489, 2001.
Redsun, M. S., Temerin, M., and Mozer, F. S.: Classification of auroral electrostatic shocks by their ion and electron associations, J. Geophys. Res., 90, 9615–9633, 1985.
Rostoker, G., Akasofu, S.-I., Foster, J., Greenwald, R. A., Kamide, Y., Kawasaki, K., Lui, A. T. Y., McPherron, R. L., and Russel, C. T.: Magnetospheric substorms – Definition and signatures, J. Geophys. Res., 85, 1663–1668, 1980.
Streltsov, A. V. and Lotko, W.: Small-scale, “electrostatic” auroral structures and Alfvén waves, J. Geophys. Res., 104, 4411–4426, 1999.
Stasiewicz, K., Khotyaintsev, Y., Berthomier, M., and Wahlund, J.-E.: Identification of widespread turbulence of dispersive Alfvén waves, Geophys. Res. Lett., 27, 173–176, 2000a.
Stasiewicz, K., Bellan, P., Chaston, C., et al.: Small scale Alfvénic structures in the aurora, Space Sci. Rev., 92, 425–533, 2000b.
Temerin, M., Boehm, M. H., and Mozer, F. S.: Paired electrostatic shocks, Geophys. Res. Lett., 8, 799–802, 1981.
Tsyganenko, N. A.: A Magnetospheric Magnetic Field Model with a Warped Tail Current Sheet, Planet. Space Sci. 37, 5–20, 1989.
Vaivads, A., André, M., Buchert, S., et al.: What high altitude observations tell us about the auroral acceleration: A cluster/DMSP conjunction, Geophys. Res. Lett., 30, 3, 1106, doi:10.1029/2002GL016006, 2003.
Wahlund, J.-E., Yilmaz, A., Backrud, M., et al.: Observations of auroral broad-band emissions by CLUSTER, Geophys. Res. Lett., 30, 11, 1563, doi:10.1029/2002GL016335, 2003.